Use of Mn doping to suppress defect sites in Ag3PO4: Applications in photocatalysis

by Admin Publikasi

Submission date: 26-Mar-2022 12:35PM (UTC+0700)
Submission ID: 1793305064
File name: APSUS-Use_of_Mn_doping-Compressed.pdf (506.68K)
Word count: 4195
Character count: 20589

Applied Surface Science 466 (2019) 352–357

Contents lists available at ScienceDirect

Applied Surface Science

journal homepage: www.elsevier.com/locate/apsusc

Full Length Article

Use of Mn doping to suppress defect sites in Ag_3PO_4: Applications in photocatalysis

Mohammad Afif[a], Uyi Sulaeman[a,*], Anung Riapanitra[a], Roy Andreas[a], Shu Yin[b]

[a] Department of Chemistry, Jenderal Soedirman University, Purwokerto 53123, Indonesia
[b] Institute of Multidisciplinary Research for Advanced Materials, Tohoku University, Sendai 980-8577, Japan

ARTICLE INFO

Keywords:
Ag_3PO_4
Defect sites
Hydroxyl defect
Mn doping
Oxygen vacancy
Photocatalysis

ABSTRACT

The highly active Mn-doped Ag_3PO_4 photocatalyst was successfully synthesized under coprecipitation method using $AgNO_3$, $Na_2HPO_4{\cdot}12H_2O$, and $MnSO_4{\cdot}H_2O$, followed by annealing. The products were characterized using the SEM, XRD, DRS, XPS, and BET. The results showed that the Mn doping decreased the broad absorption in the visible region and increased the atomic ratio of O/Ag. The hydroxyl defects and oxygen vacancies can be suppressed by Mn doping and the photocatalytic activity under visible light irradiation could be improved. This excellent photocatalytic activity was caused by decreasing the recombination of electron and holes due to suppressing the defect sites in the surface of Ag_3PO_4.

1. Introduction

The organic pollutants from the textile industry activities have led to a deterioration of the environment. Therefore, the industries should provide a sewage treatment to handle their pollutants before being sent to the environment. To realize this process, the technology of pollutant destruction using a photocatalyst could be effectively applied for the treatment of organic pollutant. The photocatalyst of TiO_2 has been widely developed to fulfill this goal. However, TiO_2 has a wide band-gap energy that can utilize only ~5% of solar energy. Therefore, another photocatalyst that has high activity under visible light could be expected.

Recently, the silver orthophosphate (Ag_3PO_4), an excellent candidate for the visible light responsive photocatalyst, has been widely studied to be applied for organic pollutant degradation, especially, for the color substances degradation. The methods of composite design [1–3], morphological design [4–7], and doping element [8–11] have been used to prepare the excellent photocatalytic activity.

The high activity of silver orthophosphate photocatalyst has been successfully synthesized using the dopant of cation [8,9], noble metal [11] and mixed anion [12]. Doping Bi^{3+} ions in the crystal can affect the valence band and band gap energy [8]. Under this preparation, Bi^{3+} ions replace P^{5+} ions in Ag_3PO_4 and suppress the hydroxyl (OH) defects on the surface. This design enhances the photocatalytic activity. The Ni^{2+} doping into Ag_3PO_4 can also affect the band gap energy and enhance the separation of electrons and holes pair [9]. The more active species are generated by Ni^{2+} doping because this ion can act as an electron acceptor that lead to the enhanced photocatalytic activity. It is very interesting that the changes of Ag_3PO_4 properties can be controlled by cation doping. The Mn (Mangan) ion, an element with many variations of oxidation number, can be applied for doping in Ag_3PO_4 photocatalyst. However, up to now, Mn ion has not yet been applied for doping in Ag_3PO_4.

Mangan ion has been effectively used as a doping element for photocatalysts. The photocatalysts of TiO_2, $SrTiO_3$, ZnO, SnO_2, and ZnS had been improved by Mn doping [13–17]. The Mn ions doped into the TiO_2 lattice can lead to a redshift of absorption and improves the photocatalytic activity [13]. The Mn^{4+} ion can also be incorporated into $SrTiO_3$ [14]. This ion can substitute the Ti^{4+} ion and shift the absorption toward the visible region. This phenomenon generates the photocatalytic reaction under the visible light irradiation. Incorporation of Mn into ZnO increases the defect site of oxygen vacancy and reduces the band gap energy [15]. This design inhibits the recombination of electrons and holes and improves the photocatalytic properties. A decreased band gap energy and crystal defect can be realized under Mn doping in SnO_2 [16] that increases the photocatalytic activity. Better photocatalytic performances of ZnS can be designed by Mn doping [17] that produces the absorption in the visible region.

Besides doping design, the defects in the lattice of a crystal can influence the photocatalytic activity. These defects can be generated by a doping element and calcination. For examples, the oxygen vacancies

* Corresponding author.
E-mail address: uyi_sulaeman@yahoo.com (U. Sulaeman).

https://doi.org/10.1016/j.apsusc.2018.10.049
Received 7 May 2018; Received in revised form 22 September 2018; Accepted 5 October 2018
Available online 06 October 2018
0169-4332/

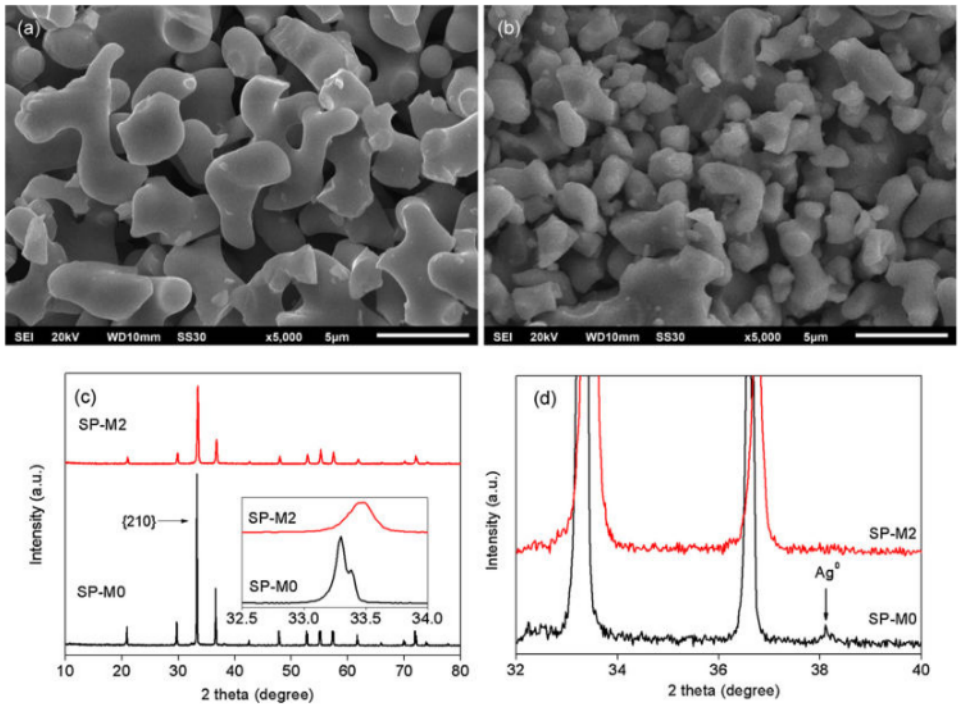

Fig. 1. SEM images of undoped Ag_3PO_4 (SP-M0) (a), Mn-doped Ag_3PO_4 (SP-M2) (b), X-ray diffraction pattern of SP-M0 and SP-M2 (c), and the enlarged XRD pattern of SP-M0 and SP-M2 (d).

in Ag_3PO_4 can be generated by calcination [18]. In a famous photocatalyst, TiO_2, the oxygen vacancies can be formed using a nanotube titanic acid that calcined at various temperatures [19]. In a certain content, the defects can enhance the activity because they increase the separation of electron-hole pairs [20]. However, a much higher defect generated on the lattice leads to being a center of recombination of holes and electrons pair that decreases the photocatalytic activity. Therefore, developing the method for controlling the defect is very useful.

Here, the Mn-doped Ag_3PO_4, for the first time, has been successfully synthesized under coprecipitation method using the starting material of $AgNO_3$, $Na_2HPO_4{\cdot}12H_2O$, and $MnSO_4{\cdot}H_2O$, followed by calcination. The results showed that the Mn doping enhanced the photocatalytic activity by suppressing the hydroxyl defect and oxygen vacancy.

2. Experimental

2.1. Synthesis of samples

The Mn-doped Ag_3PO_4 was synthesized using the coprecipitation method followed by annealing. The starting materials of $MnSO_4{\cdot}H_2O$, $AgNO_3$, $Na_2HPO_4{\cdot}12H_2O$ were used in the experiment. Typically, 1.699 g of $AgNO_3$ was dissolved in 10 ml of water (solution 1) and 1.181 g of $Na_2HPO_4{\cdot}12H_2O$ was dissolved in 20 ml of water (solution 2). The $MnSO_4$ solution (solution 3) was made by adding the $MnSO_4{\cdot}H_2O$ to the 10 ml of water. The amount variation of $MnSO_4{\cdot}H_2O$ was designed at 0.085, 0.169, 0.254, 0.338 and 0.507 g, namely, SP-M1, SP-M2, SP-M3, SP-M4, and SP-M5, respectively. The sample of undoped Ag_3PO_4 (without Mn) was also similarly made, namely SP-M0. The solution 3 was introduced to the solution 1 under magnetic stirring and then the solution 2 was slowly introduced into the mixed solution above until the yellow crystal formed. These products were dried in an oven at 105 °C for 7 h then calcined at 500 °C for 5 h.

2.2. Characterization of samples

The crystal structure was characterized using the XRD (Bruker AXS D2 Phaser). The absorptions of product and band gap energy were investigated using DRS (JASCO V-670). The morphology of the product was determined using SEM (JEOL JSM 7001F) and their specific surface areas were measured using BET (NOVA instruments). The core level of the element and binding energy were investigated using the XPS (Perkin Elmer PHI 5600).

2.3. Photocatalytic evaluation

The photocatalytic activities were investigated under visible light irradiation (LED blue light, Sanyed, 3 Watt). Amount of 0.1 g of catalyst was introduced into a 200 ml of 10 mg/L RhB solution. The distance of the sample and the lamp was designed at 10 cm. After keeping the catalyst in the dark solution to achieve the adsorption equilibrium, the photocatalytic reaction was carried out for 15 min. Four ml of sample was withdrawn at the certain interval time and centrifuged at 2000 rpm to separate the catalyst. The concentrations of RhB were measured using the spectrophotometer (Shimadzu 1800).

The reusability of photocatalyst was evaluated. After the photocatalytic reaction, the photocatalysts were recycled, washed and dried at 60 °C for 2 h. These experiments were conducted at 5 cycles.

The mechanisms of photocatalytic reaction were studied using the scavengers to trap the radical and holes under the same condition with the photocatalytic evaluation. The isopropyl alcohol (IPA), ammonium oxalate (AO) and benzoquinone (BQ) with the concentration of 0.1 mmol/L, were used to trap the hydroxyl (˙OH) radical, holes, and superoxide ion ($O_2^{-}{\cdot}$) radical, respectively [21,22].

3. Results and discussion

3.1. Characterization

The yellow Ag_3PO_4 crystals were successfully prepared using the co-precipitation of the $AgNO_3$ solution and the Na_2HPO_4 solution followed by calcination. The white solids of Ag_2SO_4 were formed after mixing the $MnSO_4$ and the $AgNO_3$ solution. These white solids disappeared by adding the Na_2HPO_4 solution to the mixed solution and the yellow solids of Ag_3PO_4 were formed. Because the solubility product constant (K_{sp}) of Ag_3PO_4 is lower than that of Ag_2SO_4, the Ag_3PO_4 can easily be precipitated. To investigate the effect of Mn doping, the undoped (SP-M0) and doped (SP-M2) samples were characterized. The bulk grains of 3–5 μm and 2–4 μm were found in SP-M0 and SP-M2 (Fig. 1(a) and (b)) with the specific surface area of 11.3 m^2/g and 17.5 m^2/g, respectively. These morphologies were formed due to the calcination at 500 °C for 7 h. The high temperature might lead to the disordered movement of fine particles leading to the bulk grains [23].

Based on the XRD results (Fig. 1(c)), the Ag_3PO_4 structure exhibits the body-centered cubic (JCPDS No. 06-0505) [2]. There are no impurities such as Ag_2SO_4 found in the samples. The diffraction peak of Mn cannot be observed, indicating that the Mn might be incorporated in a small concentration. The image of {2 1 0} diffraction peak was investigated in detail (see in the inset of Fig. 1(c)). It showed that the shifting of diffraction peak to the higher degree was observed, indicating that the Mn ions might introduce to the crystal lattice of Ag_3PO_4. The doublet of {2 1 0} diffraction peak in SP-M0 suggesting that the large defect sites in SP-M0 might be formed. The small amount of Ag^0 was observed in SP-M0, indicating that the thermal treatment generated the reduction of Ag^+ to Ag^0 (Fig. 1(d)). Incorporating the Mn into the Ag_3PO_4 suppressed the Ag^0 formation since there was no Ag^0 diffraction peak observed in SP-M2.

The absorption in the visible region (above 500 nm) of SP-M0 was larger than that of SP-M2 (Fig. 2), suggesting that the incorporation of Mn into the crystal lattice of Ag_3PO_4 may affect the optical properties of Ag_3PO_4. The large defect formed in the sample of SP-M0 might be generated by the calcination at 500 °C for 5 h. The large absorption in SP-M0 was suppressed by incorporating Mn into the Ag_3PO_4 (SP-M2). It demonstrated that the Mn doping might decrease the large defect of the surface during calcination. To investigate in detail, the band gap energies were calculated using direct optical transition [24] and showing that the 2.28 eV and 2.44 eV were found as the band gap energy of SP-M0 and SP-M2, respectively. The narrowed band gap of SP-M0 might be caused by the high defect crystal which is generated by calcination. Many researchers reported that the calcination generates the defect of oxygen vacancy [18]. After Mn doping, the band gap of Ag_3PO_4 increases to 2.44 eV which agrees with both theoretical (2.43 eV) and experimental value (2.45 eV) [25]. Based on the theory [25], the conduction band of Ag_3PO_4 is mainly attributable to Ag 5s and 5p states, whereas the valence band is dominated by O2p and Ag4d states. It is reasonable that the defect e.g. oxygen vacancy would influence the band gap energy.

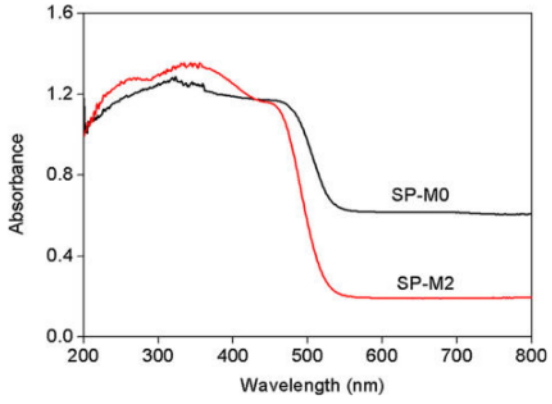

Fig. 2. The absorption spectra of undoped Ag_3PO_4 (SP-M0) and Mn-doped Ag_3PO_4 (SP-M2).

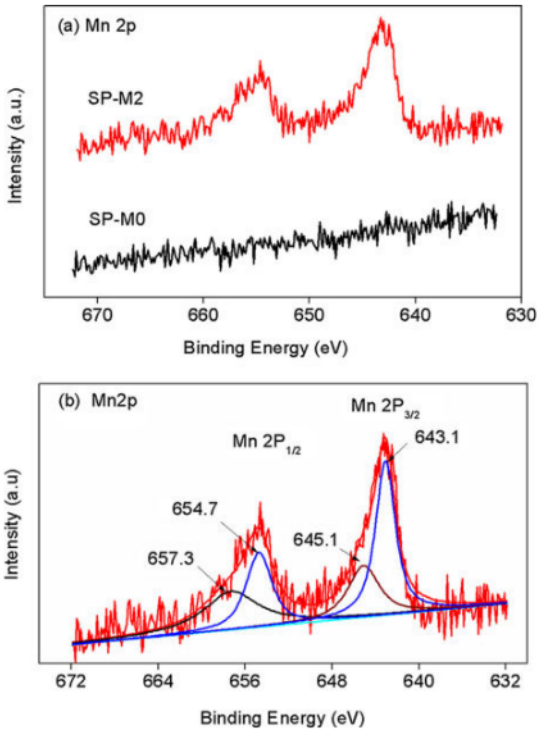

Fig. 3. The XPS of Mn 2p in undoped Ag_3PO_4 (SP-M0) and Mn-doped Ag_3PO_4(SP-M2) (a) and the deconvolution of Mn 2p in SP-M2 (b).

3.2. XPS analysis

To understand the chemical state and composition of Mn-doped Ag_3PO_4, the samples of SP-M0 and SP-M2 were deeply investigated using the XPS. The peak energy of Mn2p was clearly observed, indicating that the Mn was successfully incorporated into Ag_3PO_4 (Fig. 3(a)). The Mn doping in SP-M2 showed the atomic concentration of 2.42% (before sputtering), and 0.67% (after sputtering) as shown in Table 1. The existence of Mn after sputtering, indicating that a portion of Mn introduced to the crystal lattice of Ag_3PO_4. The XPS spectrum of Mn 2p exhibits two peaks at ca. 643.1 and 654.7 eV, which are assigned

Table 1
Surface chemical composition (%) of undoped Ag_3PO_4 (SP-M0) and Mn-doped Ag_3PO_4 (SP-M2) calculated according to XPS analysis.

Samples	Treatment	C1s	O1s	P2p	Mn2p	Ag3d	Ag/P	O/Ag
SP-M0	Before Ar^+ sputtering	16.21	50.25	12.20	0.00	21.34	1.75	2.35
	After Ar^+ sputtering	0.55	45.84	14.74	0.00	39.23	2.66	1.17
SP-M2	Before Ar^+ sputtering	14.65	50.97	11.41	2.42	20.55	1.80	2.48
	After Ar^+ sputtering	0.00	47.45	15.66	0.67	36.21	2.31	1.31

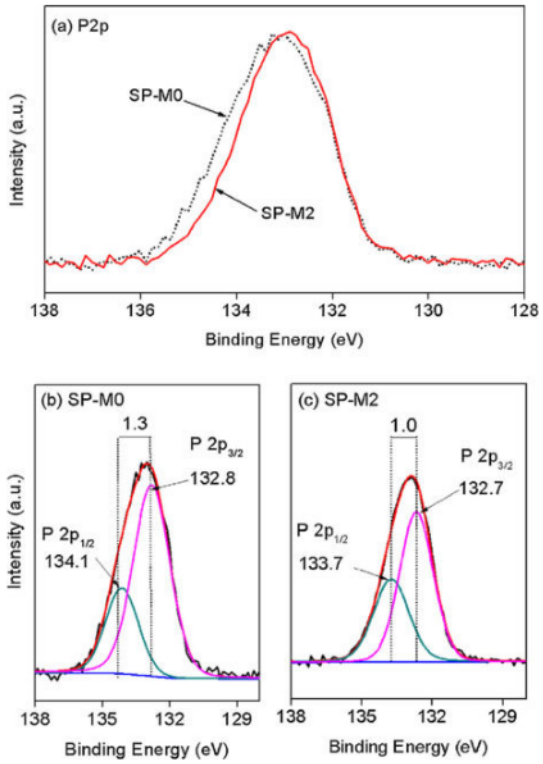

Fig. 4. The XPS of P2p for undoped Ag_3PO_4 (SP-M0) and Mn-doped Ag_3PO_4(SP-M2) (a) and their deconvolution of SP-M0 (b) and SP-M2 (c).

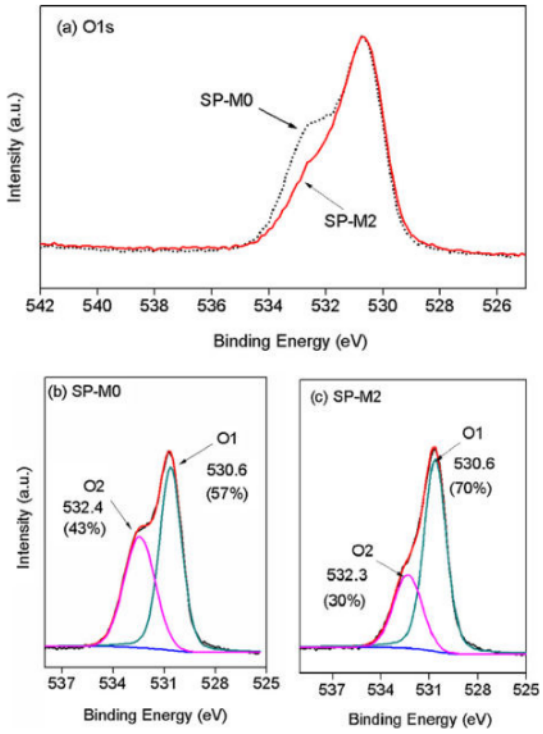

Fig. 5. The XPS of O1s for undoped Ag_3PO_4 (SP-M0) and Mn-doped Ag_3PO_4(SP-M2) (a), and their deconvolution of SP-M0 (b) and SP-M2(c).

to Mn $2p_{2/3}$ and Mn $2p_{1/2}$, respectively, with the spin-orbital splitting of 11.6 eV (Fig. 3(b)). It suggests that the manganese ions are present as Mn^{4+} [26], whereas another peak of 645.1 and 657.3 are assigned to Mn^{5+}. It is possible that the higher oxidation state of Mn could be produced during the annealing. These ions might interstitially be incorporated into Ag_3PO_4 because the ionic radius of Mn^{4+} (39 pm) and Mn^{5+} (33 pm) ions are smaller than those of Ag^+ ions (100 pm) [27]. Moreover, the atomic ratio of Ag/P in Mn-doping is significantly lower than that of the undoped after sputtering (Table 1), indicating that the Mn doping induces the Ag vacancy, therefore the Mn could easily be incorporated in the lattice of the Ag_3PO_4 crystal.

Fig. 4(a) showed that the spectra of P2p in SP-M2 exhibited the shrinkage phenomenon, indicating that the Mn affected the chemical environment of P2p. The deconvolutions of the two spectra are shown in Fig. 4(b) and (c). Two peaks of 134.1 eV and 132.8 eV are assigned to $P2p_{1/2}$ and $P2p_{3/2}$ of SP-M0, respectively with the spin-orbital splitting of 1.3 eV. Whereas, two peaks of 133.7 eV and 132.7 eV are assigned to $P2p_{1/2}$ and $P2p_{3/2}$ of SP-M2, respectively, with the spin-orbital splitting of 1.0 eV. The Mn incorporation influences the P2p environment that might decrease the spin-orbital splitting.

Fig. 5(a) shows the XPS peak energy of O1s. The deconvolution of SP-M0 and SP-M2 can be seen in Fig. 5(b) and (c), respectively. The O1s spectrum has two peaks of O1 and O2. The lower binding energy of 530.6 eV (O1) is related to O–Ag bonding and the higher binding energy of 532.4 eV is related to OH group [18]. The O2 of SP-M2 exhibits the lower ratio of intensities (30%) compared to that of SP-M0 (43%), indicating that the SP-M2 might have low OH group, whereas the SP-M0 has high OH group in the surface.

The higher intensity ratio of O2 in SP-M0 implying that the undoped Ag_3PO_4 might have large OH defects on the surface. It is similar to those of Bi^{3+} doped Ag_3PO_4 [8], the OH defects are easily created on the surface and replaced the oxygen of P–O tetrahedron due to low energy. Moreover, the high oxygen vacancy might lead to high OH defects. Large OH defects might inhibit the electron excitation and enhance the recombination by breaking the Ag–O bonds. The OH defects also increase the valence band positions and decrease the conduction band, consequently, the band gap becomes narrow. It accords to the band gap calculation from the DRS curve that shows a lower band gap in SP-M0. This phenomenon accelerates the recombination of electron and hole leading to a decreased photocatalytic ability. Because the OH defects generate excess positive charges [8] and doping Mn^{4+} also generate the positive charge, therefore doping Mn^{4+} in Ag_3PO_4 can inhibit the formation of excess OH defects due to the repulsion forces. The OH defects on the surface of Mn-doped Ag_3PO_4 (SP-M2) are significantly lower than that of undoped (SP-M0). Mn^{4+} doping might reduce the OH defects and improve the photocatalytic ability of Ag_3PO_4.

Based on Table 1, the O/Ag atomic ratio of SP-M0 is lower than that of SP-M2 both before and after sputtering, indicating that the oxygen vacancies are really formed in SP-M0. This phenomenon was also supported by the O1s spectrum as shown in Fig. 5. The intensity ratio of O1 in SP-M0 is lower that of SP-M2, suggesting that the O of O–Ag in SP-M0 is in a low concentration. After Mn doping, this detrimental Ag_3PO_4 can be repaired. In addition, the atomic ratio of Ag/P in the SP-M2 (2.31) is significantly lower than that of SP-M0 (2.66) as shown in Table 1 (after sputtering), indicating that the Mn doping also induces the silver vacancy. Therefore, the Mn doping might decrease the defect of hydroxyl radical and oxygen vacancy but increases the silver vacancy. This silver vacancy could also be a crucial role for enhanced catalytic activity. Other researchers [28,29] reported that the thermal treatment generates the silver vacancy in Ag_3PO_4. This phenomenon enhances the separation of photogenerated electrons and holes. The formation of metallic Ag during annealing process could also improve the photocatalytic activity. In our report, however, Mn doping

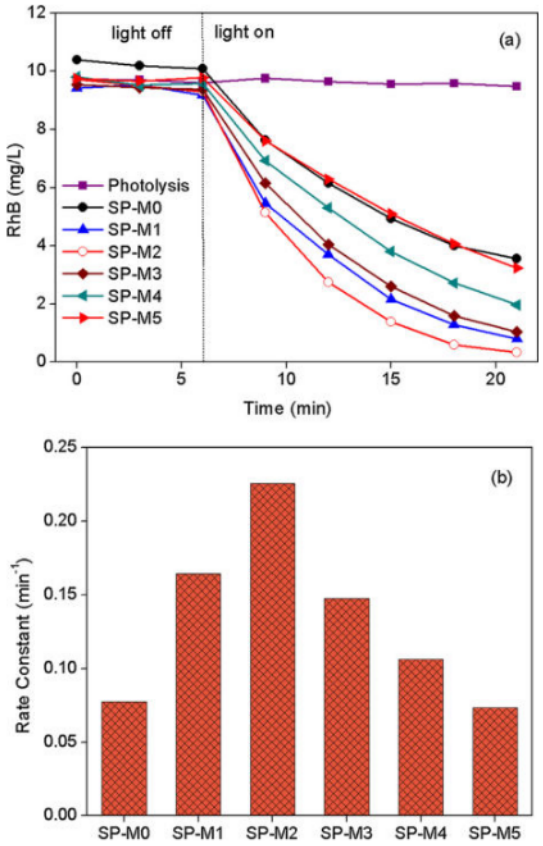

Fig. 6. Photocatalytic activities of Ag_3PO_4 with elevated concentration of doping Mn (a) and their rate constants of pseudo-first-order kinetics (b).

suppresses the formation of metallic Ag.

3.3. Photocatalytic evaluation

Fig. 6 shows the photocatalytic activity of Mn-doped Ag_3PO_4 with the variation of Mn content. The apparent pseudo-first-order kinetics equation of $\ln(C_0/C) = K_{app}t$ was used to study the rate of photocatalytic reaction, where C and C_0 are the RhB concentration at time t and zero, respectively, the K_{app} is the apparent pseudo-first-order rate constant (min^{-1}) [22,30]. The rate of photocatalytic activity has followed the pseudo-first-order kinetics, the rate constant of 0.077 min^{-1}, 0.164 min^{-1}, 0.226 min^{-1}, 0.148 min^{-1}, 0.107 min^{-1} and 0.073 min^{-1} were observed on the samples of SP-M0, SP-M1, SP-M2, SP-M3, SP-M4, and SP-M5, respectively. Incorporating the Mn into the lattice of Ag_3PO_4 affected the photocatalytic activity. The sample of SP-M2 showed the highest activity of ~2.9 times higher compared to that of SP-M0. When the concentration of Mn increases, its photocatalytic activity decreases, indicating that the high concentration of dopant might lead to a negative effect on the catalytic reaction. A too high concentration of dopant might not effectively suppress the defect site of oxygen vacancy.

To evaluate the reusability of Mn-doped Ag_3PO_4, the experiment of RhB photodegradation of SP-M0 and SP-M2 were repeated to 5 cycles (Fig. 7). The results showed that the photocatalytic activity of both SP-M0 and SP-M2 gradually decreased, indicating that the samples were not quite stable. However, the SP-M2 exhibited higher activity compared to that of SP-M0 for all cycles.

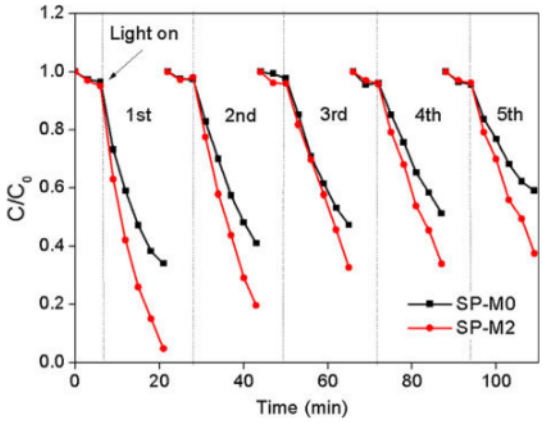

Fig. 7. The recycled photocatalytic reaction of undoped Ag_3PO_4 (SP-M0) and Mn-doped Ag_3PO_4 (SP-M2).

Mechanisms of photocatalytic reaction were studied by adding the scavengers of radicals and holes [21,22]. The IPA, AO, and BQ were added to the reaction solution as the scavenger of $^{\cdot}OH$, h^+ and $O_2^{-\cdot}$, respectively. The effect of these scavengers to the photocatalytic reaction can be seen in Fig. 8. The mechanisms of SP-M0 and SP-M2 are similar, both SP-M0 and SP-M2 are greatly suppressed by the AO and BQ, as shown in Fig. 8(a), indicating that the mechanism involve mostly

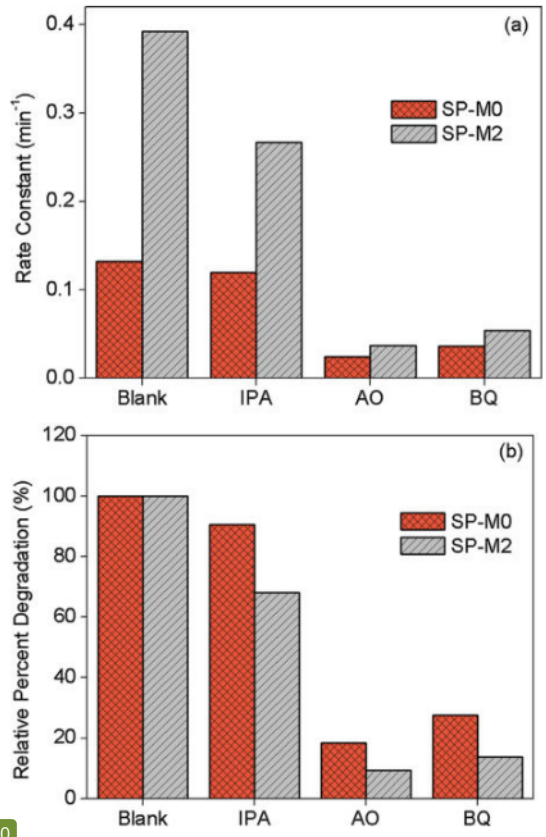

Fig. 8. The effect of scavengers on the rate constant of photocatalytic activity (a) and their relative percent degradations (b).

via h^+ and $O_2^{-\cdot}$. To understand the rate mechanism in SP-M0 and SP-M2, the rate constants of photocatalytic activity were compared to the blank one (relative percent degradation) as shown in Fig. 8(b). The results showed that relative percent degradations in SP-M2 due to scavenger of IPA, AO and BQ are lower than that of SP-M0, indicating that the role of $^{\cdot}OH$, h^+, and $O_2^{-\cdot}$ scavenger works more efficiently in SP-M2. It is because the effect of Mn doping effectively inhibits the recombination of electron and hole pairs due to suppressing the defect sites in the surface.

4. Conclusions

The Mn could be easily incorporated into the crystal lattice of Ag_3PO_4 using the coprecipitation method followed by calcination. The Mn doping decreased the broad absorption in the visible region and increased the atomic ratio of O/Ag. Large OH defect and oxygen vacancy might be generated in the sample without Mn doping during calcination. These large defects could effectively be suppressed by doping with Mn and improved the photocatalytic activity.

Acknowledgments

This research was supported by the Ministry of Research, Technology and Higher Education of the Republic of Indonesia in the Scheme of Competency Grant, Contract Number: 059/SP2H/LT/DRPM/2018. It was also partly supported by the JSPS KAKENHI Grant Number JP16H06439 (Grant-in-Aid for Scientific Research on Innovative Areas), the Dynamic Alliance for Open Innovation Bridging Human, Environment and Materials, the Cooperative Research Program of "Network Joint Research Center for Materials and Devices".

References

[1] T. Zhou, G. Zhang, P. Ma, X. Qiu, H. Zhang, H. Yang, G. Liu, J. Alloys Compd. 735 (2018) 1277–1290.
[2] X. Cui, L. Tian, X. Xian, H. Tang, X. Yang, Appl. Surf. Sci. 430 (2018) 108–115.
[3] H. Wang, L. Zou, Y. Shan, X. Wang, Mater. Res. Bull. 97 (2018) 189–194.
[4] U. Sulaeman, F. Febiyanto, S. Yin, T. Sato, Catal. Commun. 85 (2016) 22–25.
[5] L. Wang, L. Wang, D. Chu, Z. Wang, Y. Zhang, J. Sun, Catal. Commun. 88 (2017) 53–55.
[6] C. Zheng, H. Yang, Y. Yang, J. Ceram. Soc. Jpn. 125 (2017) 141–144.
[7] R. Guo, Y. Fan, Y. Tang, RSC Adv. 7 (2017) 23977–23981.
[8] S. Zhang, S. Zhang, L. Song, Appl. Catal. B 152–153 (2014) 129–139.
[9] L. Song, Z. Chen, T. Li, S. Zhang, Mater. Chem. Phys. 186 (2017) 271–279.
[10] M.S.A. Hussien, I.S. Yahia, J. Photochem. Photobiol. A 356 (2018) 587–594.
[11] T. Yan, H. Zhang, Y. Liu, W. Guan, J. Long, W. Li, J. You, RSC Adv. 4 (2014) 37220–37230.
[12] W. Cao, Z. Gui, L. Chen, X. Zhu, Z. Qi, Appl. Catal. B 200 (2017) 681–689.
[13] Q.R. Deng, X.H. Xia, M.L. Guo, Y. Gao, G. Shao, Mater. Lett. 65 (2011) 2051–2054.
[14] G. Wu, P. Li, D. Xu, B. Luo, Y. Hong, W. Shi, C. Liu, Appl. Surf. Sci. 333 (2015) 39–47.
[15] N.A. Putri, V. Fauzia, S. Iwan, L. Roza, A.A. Umar, S. Budi, Appl. Surf. Sci. 439 (2018) 285–297.
[16] B. Babu, A.N. Kadam, G.T. Rao, S.W. Lee, C. Byond, J. Shim, J. Lumin. 195 (2018) 283–289.
[17] L. Wang, P. Wang, B. Huang, X. Ma, G. Wang, Y. Dai, X. Zhang, X. Qin, Appl. Surf. Sci. 391 (2017) 557–564.
[18] R. Chong, X. Cheng, B. Wang, D. Li, Z. Chang, L. Zhang, Int. J. Hydrogen Energy 41 (2016) 2575–2582.
[19] L. Hou, M. Zhang, Z. Guan, Q. Li, J. Yang, Appl. Surf. Sci. 428 (2018) 640–647.
[20] J. Yan, G. Wu, N. Guan, L. Li, Z. Li, X. Cao, Phys. Chem. Chem. Phys. 15 (2013) 10978–10988.
[21] W. Liu, M. Wang, C. Xu, S. Chen, X. Fu, Mater. Res. Bull. 48 (2013) 106–113.
[22] U. Sulaeman, D. Hermawan, R. Andreas, A.Z. Abdullah, S. Yin, Appl. Surf. Sci. 428 (2018) 1029–1035.
[23] V. Stengl, S. Bakardjieva, N. Murafa, V. Houskova, K. Lang, Microporous Mesoporous Mater. 110 (2008) 2575–2582.
[24] M.A. Butler, J. Appl. Phys. 48 (1977) 1914–1920.
[25] J.J. Liu, X.L. Fu, S.F. Chen, Y.F. Zhu, Appl. Phys. Lett. 99 (2011) 191903.
[26] Q. Li, G. Li, C. Fu, D. Luo, J. Fan, D. Xie, L. Li, J. Mater. Chem. A 3 (2015) 10592–10602.
[27] R.D. Shannon, Acta Cryst. A32 (1976) 751–767.
[28] T. Yan, W. Guan, J. Tian, P. Wang, W. Li, J. You, B. Huang, J Alloys Compd. 680 (2016) 436–445.
[29] T. Yan, W. Guan, Y. Xiao, J. Tian, Z. Qiao, H. Zhai, W. Li, J. You, Appl. Surf. Sci. 391 (2017) 592–600.
[30] Y. Li, X. Li, J. Li, J. Yin, Water Res. 40 (2006) 1119–1126.

Use of Mn doping to suppress defect sites in Ag3PO4: Applications in photocatalysis

ORIGINALITY REPORT

13%	6%	13%	2%
SIMILARITY INDEX	INTERNET SOURCES	PUBLICATIONS	STUDENT PAPERS

PRIMARY SOURCES

1	Uyi Sulaeman, Suhendar Suhendar, Hartiwi Diastuti, Anung Riapanitra, Shu Yin. "Design of Ag3PO4 for highly enhanced photocatalyst using hydroxyapatite as a source of phosphate ion", Solid State Sciences, 2018 Publication	4%
2	Uyi Sulaeman, Dadan Hermawan, Roy Andreas, Ahmad Zuhairi Abdullah, Shu Yin. "Native defects in silver orthophosphate and their effects on photocatalytic activity under visible light irradiation", Applied Surface Science, 2018 Publication	2%
3	Sulaeman, Uyi, Xiaoyong Wu, Bin Liu, Shu Yin, and Tsugio Sato. "Synthesis of Ag3PO4-polyvinyl alcohol hybrid microcrystal with enhanced visible light photocatalytic activity", Applied Surface Science, 2015. Publication	1%

4	M. Afif, J.P. Girardeau-Montaut, C. Tomas, C. Girardeau-Montaut, K. Warda, J. Delafond, C. Fayoux. "Ultrashort electron emission improved by alkali ions implantation into metallic photocathodes", Applied Surface Science, 1997 Publication	1 %
5	Submitted to International School of Bydgoszcz Student Paper	1 %
6	Myung Jong Kang, Hyejin Yu, Wonjoo Lee, Hyun Gil Cha. "Efficient Fe2O3/C-g-C3N4 Z-scheme heterojunction photocatalyst prepared by facile one-step carbonizing process", Journal of Physics and Chemistry of Solids, 2019 Publication	1 %
7	daneshyari.com Internet Source	1 %
8	Uyi Sulaeman, Xiaoyong Wu, Bin Liu, Shu Yin, Tsugio Sato. "Synthesis of Ag 3 PO 4 -polyvinyl alcohol hybrid microcrystal with enhanced visible light photocatalytic activity", Applied Surface Science, 2015 Publication	1 %
9	Riapanitra, Anung, Intan Futihah, Uyi Sulaeman, Shu Yin, and Tsugio Sato. "The Role	1 %

of Fe^{2+} Ions on the Photocatalytic Reaction of Ag_3PO_4 for Rhodamine B Degradation", Advanced Materials Research, 2015.
Publication

10	"Facile Synthesis, Characterization and Visible-Light Photocatalytic Performance of Ag3PO4", Asian Journal of Chemistry, 2014. Publication	1 %
11	Sulaeman, Uyi, Estri Yunari, Ponco Iswanto, Shu Yin, and Tsugio Sato. "Synthesis of Bi_2O_3/Ag_3Po_4 Composites and their Photocatalytic Activities under Visible Light Irradiation", Advanced Materials Research, 2015. Publication	1 %
12	Sulaeman, Uyi, Hesti Pratiwi, Anung Riapanitra, Ponco Iswanto, Shu Yin, and Tsugio Sato. "Hydrothermal Synthesis and Photocatalytic Properties of $BiPO_4/Ag_3PO_4$ Heterostructure for Phenol Decomposition", Advanced Materials Research, 2014. Publication	1 %

Exclude quotes	Off	Exclude matches	< 1%
Exclude bibliography	On		